






# Provenance and transport of supraglacial debris revealed by variations in debris geochemistry on Khumbu Glacier, Nepal Himalaya

Martin P. Kirkbride<sup>1</sup>  | Sophie C. Sherriff<sup>1,2</sup> | Ann V. Rowan<sup>3</sup>  |  
David L. Egholm<sup>4</sup> | Duncan J. Quincey<sup>5</sup>  | Evan Miles<sup>6</sup> | Bryn Hubbard<sup>7</sup>  |  
Katie Miles<sup>7</sup> 

<sup>1</sup>Earth, Energy and Environment, University of Dundee, Dundee, Scotland, UK

<sup>2</sup>Wessex Water, Bristol, UK

<sup>3</sup>Department of Earth Science, University of Bergen and Bjerknes Centre for Climate Research, Bergen, Norway

<sup>4</sup>Department of Geoscience, Aarhus University, Aarhus, Denmark

<sup>5</sup>School of Geography, University of Leeds, Leeds, UK

<sup>6</sup>Swiss Federal Institute for Forest, Snow, and Landscape Research WSL, Birmensdorf, Switzerland

<sup>7</sup>Centre for Glaciology, Department of Geography and Earth Sciences, Aberystwyth University, Aberystwyth, Wales, UK

## Correspondence

Kirkbride MP, Earth, Energy and Environment, University of Dundee, Dundee DD1 4HN, Scotland, UK.

Email: [m.p.kirkbride@dundee.ac.uk](mailto:m.p.kirkbride@dundee.ac.uk)

## Funding information

Quaternary Research Association; Royal Society, Grant/Award Number: R1; Aberystwyth University, Grant/Award Numbers: P002021, P00265X

## Abstract

The origin of supraglacial debris covers is often conceptualised as the formation of a surface lag by melt-out of englacial debris from slow-moving ice, where complexity arises from feedback between debris thickness and sub-debris ice melt. Here, we examine the origin of a debris cover from the perspective of debris provenance and changing tributary supply in a high-elevation compound valley glacier. Geochemical analysis of 11 major elements in 21 debris samples from six tributaries of Khumbu Glacier (Nepal) shows unambiguous statistical differentiation of debris sources reflecting lithological differences between tributary catchments. Twenty-four samples from transects across the ablation area are partitioned according to their source areas using the FR2000 sediment unmixing model. We estimate the age of ice at each transect using a higher order ice flow model. The results show greater proportions of debris from lateral tributaries in downglacier locations that have experienced longer flowline histories. More recently, ice from the Main Himalayan Divide (Western Cwm) has become relatively more important. This suggests a change in the state of the lower glacier's structure depending on the relative ice discharges of lateral and divide sources. Ice flux from lower elevation tributaries was more important probably prior to a weakening of the Indian Summer Monsoon at around 1420 CE. The lower elevation tributaries lie within the range of late Holocene equilibrium line altitude variation and therefore respond most sensitively to climatic drivers of the glacier's flow structure. Negative glacier mass balance since around 1900 CE caused tributary glaciers to detach and high-elevation catchments to re-establish as the dominant ice source to Khumbu Glacier.

## KEYWORDS

geochemical fingerprinting, glacier response, ice flow model, Khumbu Glacier, sediment unmixing model, supraglacial debris

## 1 | INTRODUCTION

Debris-covered glaciers are widespread in high mountain ranges and their debris mantles are potentially a valuable record of catchment denudation (Herreid & Pellicciotti, 2020; Scherler & Egholm, 2020). In

geologically varied mountains, supraglacial debris on compound valley glaciers comprises flow-parallel units with distinctive lithological compositions. These sediment stores can be used to estimate denudation rates (Scherler & Egholm, 2020; Ward & Anderson, 2011; Wetterauer et al., 2022).

This is an open access article under the terms of the [Creative Commons Attribution-NonCommercial](https://creativecommons.org/licenses/by-nc/4.0/) License, which permits use, distribution and reproduction in any medium, provided the original work is properly cited and is not used for commercial purposes.

© 2023 The Authors. *Earth Surface Processes and Landforms* published by John Wiley & Sons Ltd.

Tributary glaciers of varied elevations and geometries have different sensitivities to climate change resulting in unsynchronised variations in ice and debris fluxes into the glacier tongue (Rowan et al., 2015). An interesting and unexplored question is whether such debris-covered tongues preserve an archive of ice flux from their tributaries. Lateral variation in ice discharge is well known in surge-type valley glaciers where distinctive medial moraine loops demarcate the changing widths of flow units (e.g., Kristensen & Benn, 2012) and also demonstrate how flow units from surging tributaries are advected downglacier. We suggest that a similar climatically driven process occurs in the absence of surging over longer timescales and with more subtlety, such that evidence of its effect is rarely detected.

Most provenance surveys of glacial sediments have been carried out on till deposits, mainly for ore mineral prospecting purposes (see review by McClenaghan & Paulen, 2018), whereas there are few studies on active glaciers. DiLabio and Shilts (1978) used the elemental composition of englacial debris bands to determine the transport distances of entrained basal debris beyond geological boundaries in the Canadian Arctic. Stephens et al. (1990) sampled heavy minerals in the medial moraines of two compound Alaskan glaciers to identify geochemically anomalous zones in headwater cirques. These two studies demonstrated that the geochemical signatures of tributary glacier source areas were preserved in both the englacial and supraglacial transport zones over tens of kilometres of transport. There are no previous studies of geochemical patterns in supraglacial debris covers in the Himalaya, where the influence of both the topographic and

climatic settings on glacier evolution over centennial timescales is poorly understood (Scherler et al., 2011).

This study investigates the composition of the supraglacial debris layer of Khumbu Glacier, Nepal (Figure 1), in relation to the geology of contributing tributary catchments. Geochemical fingerprinting allows the reconstruction of changing ice and debris fluxes from contributing tributaries, and assessment of the extent to which debris cover has been reworked by local mass movement and supraglacial streams (Bartlett et al., 2021).

## 2 | DEBRIS DISPERSAL PROCESSES IN COMPOUND VALLEY GLACIERS

To interpret how debris from multiple tributary glaciers is dispersed throughout a supraglacial debris mantle, it is necessary to understand how the structure of a compound glacier tongue determines debris delivery to the glacier surface. The summary provided here is expanded and systematised in the [Supplementary Material](#).

Debris dispersal includes primary dispersal, which refers to the migration of debris band outcrops across melting ice surfaces (Kirkbride & Deline, 2013), and secondary dispersal by redistribution of debris down slopes and by supraglacial streams (Bartlett et al., 2021). The geometry of confluence zones determines the disposition of englacial debris septa within the glacier tongue (Figure 2) and therefore sets the pattern of primary dispersal by melt-out at the

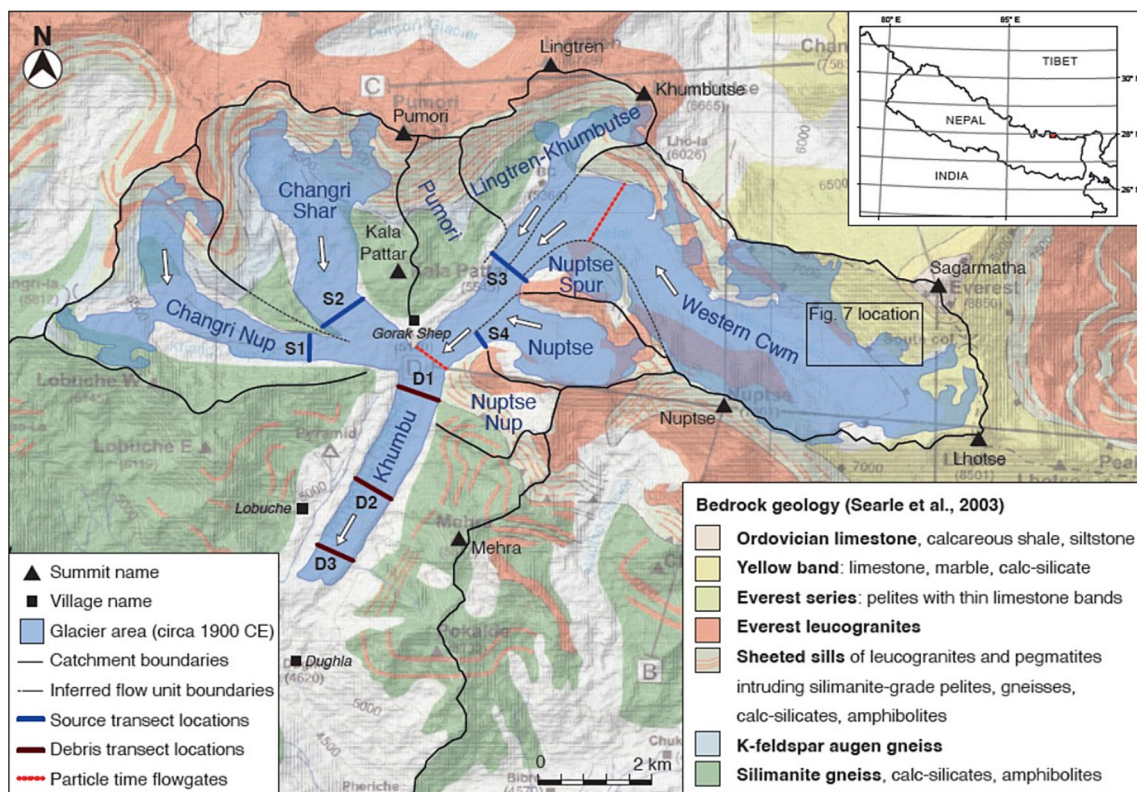
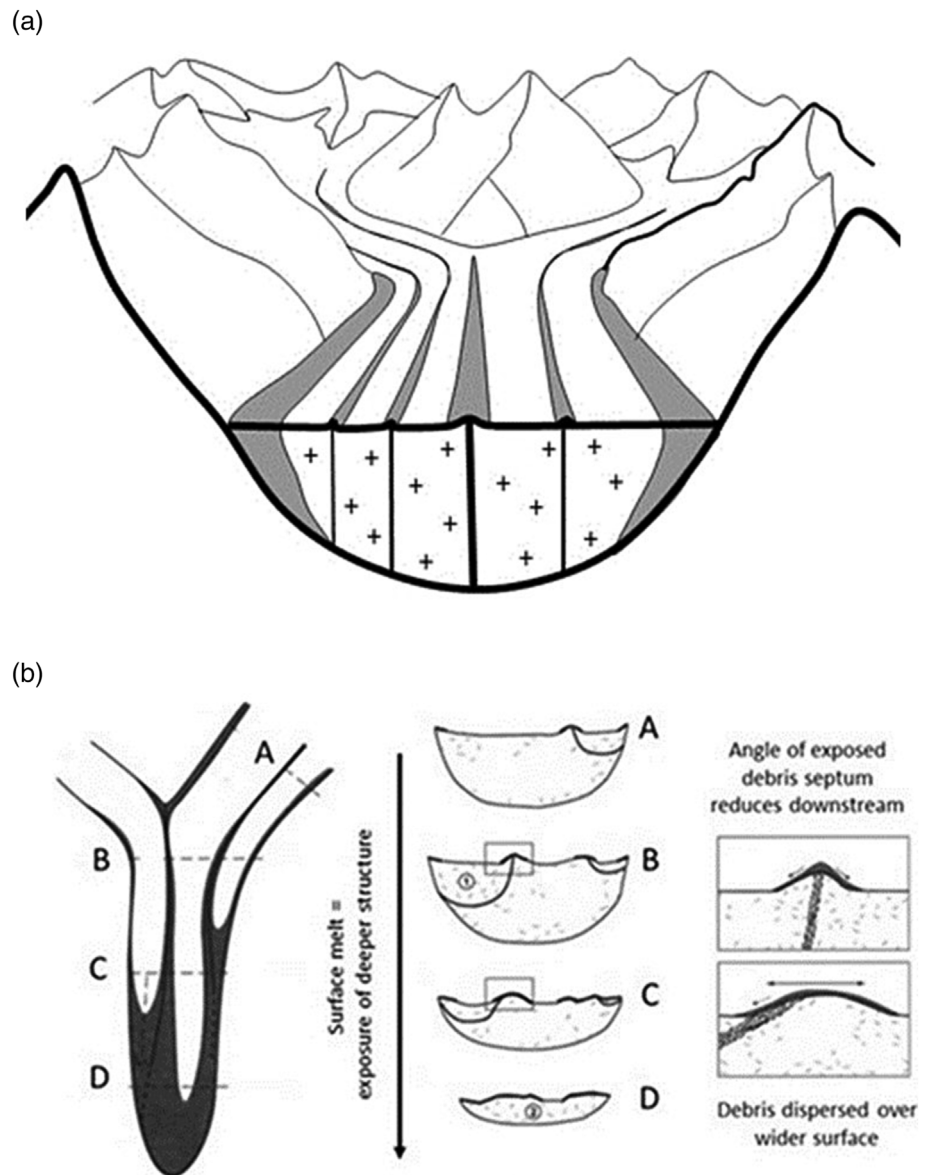


**FIGURE 1** Map of Khumbu Glacier showing the bedrock geology after Searle et al. (2003) overlain on a shaded relief map from the 8 m HMA DEM (Shean, 2017) and the debris source areas employed in the FR2000 unmixing model. The transects sampled to fingerprint the source area geochemistry are labelled S1–S4 (blue lines), the transects from the debris-covered glacier tongue are D1–D3 (brown lines), and the flowgates used to calculate glacial debris transport times are red lines. The Inset map shows the location of Khumbu Glacier in Nepal. The glacier outline is taken from the RGI v.5 and is intended to represent the early 20th-century configuration of the Khumbu Glacier before the detachment of the Changri Glacier tributary.

**FIGURE 2** Schematic diagram of structures of a tributary confluence zone and the formation of ice flow units in a compound glacier tongue. (a) Vertical debris septa generated by full-depth tributary junctions (after Scherler & Egholm, 2020). (b) The likely structure where tributaries enter from hanging valleys, causing primary dispersal of debris (see Kirkbride & Deline, 2013). Here, sections A–D show the downstream emergence of englacial debris septa at lower angles causing lateral spreading of supraglacial debris as the tributary flow unit ablates away. Note that ice from a minor tributary may ablate completely upstream of the main glacier terminus, but its residual debris will continue to be transported downglacier.



surface. As confluent ice flow units are thinned by surface ablation, they become narrower and their bounding debris septa outcrop at lower angles and are therefore more able to migrate laterally. Melt-out debris accumulates on the glacier surface in bands whose widths reflect the original width of the confluent flow, less any dynamic lateral compression (Figure 2). Field mapping of these bands in continuous debris mantles is difficult where distinctive lithological stripes are absent.

Along flow unit margins, greater englacial debris concentrations melt out to give greater supraglacial layer thickness within medial moraines, which wax downstream by differential ablation (Anderson, 2000; Mölg et al., 2020; Small & Clark, 1974). Secondary transport involves the gravitational motion of debris down the steepening lateral moraine flanks. Along inter-moraine troughs, supraglacial streams entrain debris and clast rounding is rapid in high-energy transport. Fluvially transported debris is widespread in the lower glacier tongue both in relict channels and conduit fills of sorted sand and gravel (Figure S1) and within extensive areas of debris cover (Figures S2 and S3).

Primary and secondary dispersal processes (Table S1) are hypothesised to influence the strength and pattern of geochemical

matching between debris sources and debris on the lower glacier tongue. An a priori understanding of these processes is a pre-requisite for interpreting the geochemical results presented below.

### 3 | STUDY AREA

#### 3.1 | Khumbu Glacier

Khumbu Glacier (Sagarmatha National Park, Nepal) is a summer (monsoonal)-accumulation debris-covered compound valley glacier 16 km long and 19 km<sup>2</sup> in area. The glacier drains both the Main Himalayan Divide, at elevations ranging from 6006 to 8848 m above sea level (a.s.l.), and several tributary catchments to the south surrounded by peaks reaching 7000 m. Two tributaries currently join the main tongue of Khumbu Glacier, but in recent centuries up to seven tributaries were connected (Figure 1). The ablation area of Khumbu Glacier is heavily debris-covered over a length of 11 km and an area of 7 km<sup>2</sup> (Figure 3). The lower tongue terminates at ~4920 m a.s.l. and is confined by large ice-marginal moraines constructed over the last 8 ka (Hambrey et al., 2008; Hornsey et al., 2022).

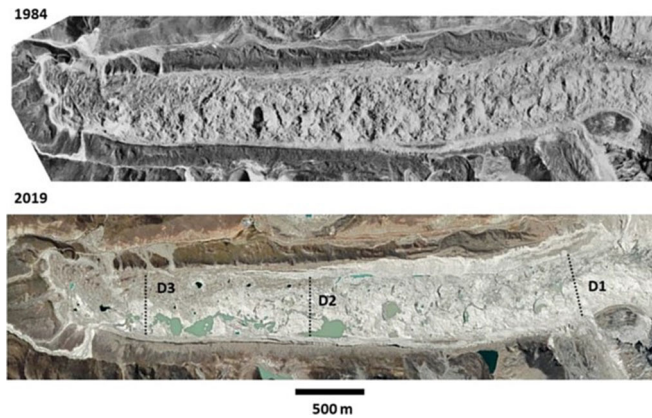


**FIGURE 3** Aerial photography illustrating changes to the surface morphology of Khumbu Glacier over a 25 year interval from 1984 CE to 2019 CE. Note the absence of supraglacial streams and paucity of surface ponds in 1984 CE and the development of a linked stream-pond system by 2019 CE. Transects sampled for major elements in April–May 2018 CE are indicated in the later image.

Multidecadal change at Khumbu Glacier has involved surface elevation change in the ablation zone of  $-0.48 \pm 0.11$  m w.e.  $a^{-1}$  from 2009–2018 (Bolch, Buchroithner, Pieczonka, & Kunert, 2008; King et al., 2017; King, Bhattacharya, et al., 2020; Nuimura et al., 2012) which has resulted in reduced surface slope (Bolch et al., 2011) and velocity leading to terminal stagnation (Haritashya et al., 2015; Nakawo et al., 1999; Quincey et al., 2009; Scherler et al., 2008), expansion of supraglacial debris (Bolch, Buchroithner, Peters, et al., 2008; Seko et al., 1998), and supraglacial ponds (Sakai et al., 2000; Bolch, Buchroithner, Pieczonka, & Kunert, 2008; Benn et al., 2012; Nuimura et al., 2012; Watson et al., 2016; Miles et al., 2020). The pattern of change at Khumbu Glacier is governed by a downglacier increase in debris thickness with thinning focused around the transition zone to stagnant ice and an upstream increase in debris-covered area. This developmental path is predicted to result in the complete separation of the stagnant debris-covered tongue from the active glacier in the next few decades (Naito et al., 2000; Rowan et al., 2021). Reconstructions of glacier flow structure made in this paper are based around glacier configurations which existed prior to the late 20th-century thinning and stagnation, and do not include the recent strongly negative trend.

### 3.2 | Bedrock geology in the Khumbu Valley

There is a broad-scale geological contrast between headwalls surrounding the high accumulation zones of Khumbu Glacier and lower ranges south of the Main Divide and Nuptse ridge (Figure 1) that facilitates a geochemically based provenance approach. The main tributaries of Khumbu Glacier drain cirques cut into varied sedimentary and crystalline lithologies (Searle et al., 2003). The Himalayan Main Divide and the Nuptse ridge comprise sillimanite-grade pelites intruded extensively by the Everest leucogranites, above bulbous intrusions of leucogranite which contain Na and K feldspar, muscovite, biotite, tourmaline and garnet. The northern and eastern headwalls of the Western Cwm comprise Everest Series pelites and sedimentary limestones and calc-silicate rocks, above which the low-

angle Qomolangma Detachment separates the summit rocks of Sagarmatha (Everest) comprising Ordovician limestones, shales and siltstone, clast of which rapidly disintegrate in the supraglacial debris cover. These lithologies were emplaced above the Lhotse Detachment over a suite of metamorphic lithologies dominated by sillimanite gneiss, metapelites, calc silicates and amphiboles. These form the Lobuche massif west of Khumbu Glacier and are overlooking the south margin of Changri Nup Glacier, the lower slopes of Pumori and the Mehra–Pokalde ridge to the east. A band of K-feldspar augen gneiss traverses the base of the headwalls of Changi Shar and Changri Nup Glaciers.

### 3.3 | Debris source areas to Khumbu Glacier

Tributary catchments contributing debris and ice to Khumbu Glacier fall into three groups (Figure 1): (1) western sources that include Changri Shar, Changri Nup and Pumori Glaciers; (2) eastern sources that include Nuptse Glacier and the informally named Nuptse Nup cirque; and (3) the Lingtren–Khumbutse wall and Western Cwm on the Main Divide. These catchments range in area between 2.0 and 18.5 km<sup>2</sup> and between 1750 and 2950 m in local relief (Table 1). Pumori and Nuptse Nup glaciers were not sampled due to logistical constraints. Pumori Glacier (Figure 1) was a tributary in the Little Ice Age (LIA), which supplied leucogranite, sillimanite gneiss and schist based on mapped geology (Searle et al., 2003). Nuptse Nup cirque was formerly confluent with the main glacier tongue after the formation of the main lateral moraine dated to  $1.3 \pm 0.1$  ka (Hornsey et al., 2022) and would have supplied mainly sillimanite schist and gneiss to the eastern margin of Khumbu Glacier.

The Holocene Changri Nup Glacier formerly comprised two distinct tributaries that joined above a single confluence with Khumbu Glacier. Debris from Changri Shar Glacier was sourced from the partially glacierised headwalls of a large cirque west of Pumori comprising leucogranite sills and late-phase pegmatite intrusions into gneisses above the Khumbu Thrust (Searle et al., 2003). Changri Nup Glacier receives debris from two cirques to the southwest, the major headwall sources comprising similar leucogranites and gneisses, but with extensive cliffs of predominantly biotite and sillimanite-rich schist and gneiss outcropping at a lower structural level and forming the southern wall of the valley.

East of Pumori, the Lingtren–Khumbutse wall is composed of leucogranite and schist. This leads eastwards above the Khumbu Icefall into the high Western Cwm, supplying debris from the faces of Everest, Lhotse and Nuptse. This debris forms a dark lithological band emerging below the icefall, derived from Everest Series lithologies. A parallel flow unit below the icefall contains leucogranite/gneiss sourced from the northwest spur and north face of Nuptse. A major tributary is the western cirque of Nuptse where a 2000-m-high headwall supplies a flow unit directly into the eastern margin of the Khumbu Glacier tongue, bounded by a pronounced medial moraine.

## 4 | METHODS

We used a sediment fingerprinting model applied to x-ray fluorescence (XRF) analyses of major element relative concentrations in

**TABLE 1** Details of sampled transects on Khumbu Glacier.

Transect and code	Samples	Start co-ordinates	End co-ordinates	Catchment area (km <sup>2</sup> )	Catchment relief (m)	Transect altitude (m)
<b>Source samples</b>						
Changri Nup S1	S1-1 to S1-4	27.97818°N 86.81238°E	27.97548°N 86.81273°E	13.75	c. 5100–6853	5134–5171
Changri Shar S2	S2-1 to S2-4	27.98035°N 86.81515°E	27.98360°N 86.82047°E	13.00	c. 5100–7145	5153–5162
Lingtren/Khumbutse S3	S3-7 to S3-8	27.99222°N 86.84362°E	27.99200°N 86.8427°E	9.75	c. 5500–7145	5162–5179
Western Cwm S3	S3-2 to S3-6	27.99082°N 86.84795°E	27.99230°N 86.8449°E	18.50	c. 5900–8848	5168–5173
Nuptse spur S3	S3-1	27.99027°N 86.84862°E	n/a	4.00	c. 5200–7400	5195
Nuptse cirque S4	S4-1 to S4-4	27.97830°N 86.8413°E	27.98032°N 86.83988°E	3.25	c. 5100–7600	5076–5104
<b>Debris samples</b>						
Upper tongue D1	D1-1 to D1-8	27.96864°N 86.83134°E	27.97010°N 86.82686°E			5013–5035
Middle tongue D2	D2-1 to D2-8	27.95082°N 86.8175°E	27.94922°N 86.82045°E			4902–4921
Lower tongue D3	D3-1 to D3-8	27.93978°N 86.8101°E	27.93693°N 86.8153°E			4888–4903

supraglacial debris (Sherriff et al., 2015) in combination with a higher order ice flow model of debris transport pathways (Scherler & Egholm, 2020). Debris provenance was identified using the FR2000 sediment unmixing model (Franks & Rowan, 2000), which statistically unmixes the major elements in supraglacial debris samples from the glacier tongue (termed debris samples) and matches these to the relative contributions of debris from geochemically fingerprinted tributary catchments (termed source samples). By mapping geochemical variation across the debris-covered glacier tongue there is potential to identify where debris was derived from tributaries that are no longer contiguous with the glacier tongue and to identify tributaries which have previously contributed more or less debris (and, by proxy, ice). Transects to sample supraglacial debris were chosen from each source area to determine the geochemical composition of their contributing area and at three locations on the main tongue of Khumbu Glacier to determine the changing composition of the supraglacial debris layer with distance towards the terminus.

#### 4.1 | Sampling strategy

Source samples were collected along transects labelled S1 to S4 across glacier flow units draining tributary catchments close to their junctions with the compound tongue of Khumbu Glacier (Figure 1). Between four and eight sediment samples were collected from each transect. Three transects across the debris-covered glacier tongue were named 'debris' transects D1, D2 and D3 (Table 1). Eight sediment samples were collected from each transect on the tongue with a mean spacing of 55 m between sampling points (range 29–82 m). Each sample consisted of 150–200 g dry debris collected 0.1 m below the debris surface and sieved to remove the <250 and >2000 µm fractions. The finer fraction was removed to guard against sample

contamination by aeolian deposition. Samples were located using a hand-held Garmin GPS. In the laboratory, each sample was split and subsamples were (a) dried and analysed for loss-on-ignition, (b) analysed for granulometry using a Beckman-Coulter LS13-320 laser sizer and (c) analysed for major element chemistry using a mounted Olympus Delta Professional XRF detector.

#### 4.2 | Major element geochemistry

The geochemistry of sediment samples was analysed for 34 elements Mg, Al, Si, P, S, K, Ca, Ti, V, Cr, Mn, Fe, Co, Ni, Cu, Zn, As, Se, Rb, Sr, Y, Zr, Nb, Mo, Ag, Cd, Sn, Sb, W, Hg, Pb, Bi, Th and U. Data were also collected for the proportion of light elements, a combined parameter representing elements whose concentration cannot be formally measured using XRF. Each element represents a potential tracer of debris provenance. Samples were pre-treated to remove organic matter and were chemically and physically disturbed before analysis (following the protocol of Sherriff et al., 2015). The specific surface area of the source and debris samples was analysed by laser diffraction. Organic matter content was determined by loss on ignition. All elemental concentration data were then individually corrected for particle size and organic matter concentration following Sherriff et al. (2018).

#### 4.3 | Sediment unmixing modelling

Source samples were grouped into a six-source and a combined three-source model and the unmixing model run for both groups. The three-source model combines the individual sources areas of Changri Shar and Changri Nup, Nuptse spur and Nuptse cirque, and the

Western Cwm with the Lingtren-Khumbutse source into coarser groups to investigate fundamental patterns of changing supply between east, west and northern tributaries. The rationale for limiting the analysis to three sources was that it would increase statistical differentiation and provide a coarser but tractable level of interpretation. The six-source model provided a more refined interpretation of glacier change but at the cost of potentially weaker source area distinction and interpretive ambiguities. The 24 debris samples from the tongue are individually matched to likely source areas. The model determined from the mix of major elements in each sample the proportion of sediment originating from each source.

Unmixing for sediment fingerprinting analysis was performed on qualifying tracer elements following a selection procedure. Firstly, the non-parametric Kruskal–Wallis test determined the ability of each tracer to distinguish between at least two sediment sources and an element was retained when  $p \leq 0.05$ . Secondly, to remove tracers displaying non-conservative behaviour (where the measured range of an element's concentration lies outside the range of that element in the source samples), tracer concentrations of debris cover samples were assessed against the corresponding range in the source dataset. Where debris sample element concentrations lay beyond the range of source sample values, the tracer was highlighted as having higher uncertainty. Finally, the combined discrimination capability of the remaining tracer set to successfully assign source samples to their correct group was assessed using a multiple discriminant analysis for each debris sample.

The FR2000 model was employed to ascertain the mean and 95th percentile contributions of sediment sources to each tongue sample from probability distributions. The FR2000 algorithm approach for unmixing samples for source identification is summarised in Franks and Rowan (2000). The impact of uncertainty in the sample means on source contributions is propagated using Monte Carlo sampling. A mean probability distribution for each tracer value at source and sink is derived from the input dataset from which the median source contribution is estimated and 95% confidence intervals are reported from the resultant frequency distribution.

Initially, debris samples were statistically unmixed against all potential sources (Table 2) to identify variability in dominant sources across the glacier tongue. Unlike fluvial studies, where complete redistribution of sediments is generally assumed across a hydraulic cross-section, laminar flow in glaciers maintains longitudinal flow units along the glacier. As such, for transect D1, potential sediment sources for specific samples were minimised based on their location, and relevant sources for each sample were identified by the delineation of transport pathways on aerial photographs. For samples D1-1 to D1-4, the model prevented potential contributions from Changri Valley sources (transects S1 and S2) from reaching the eastern part of the glacier. Similarly, for sample D1-8, Nuptse sources S4 were removed from the analysis, and un-mixing including sources S1, S2 and S3 was performed. We allow greater cross-sectional mixing in transects D2 and D3, in which the model allowed all six sources to deliver debris to tongue samples along the length of these transects to capture the effect of possible mixing by reworking processes.

#### 4.4 | Adjustments for unsampled source areas

The FR2000 model can only allocate debris samples from transects D1 to D3 to sampled source areas. Because two sources (Pumori and Nuptse Nup) were not sampled in the field, the model mismatched debris from these sources to other fingerprinted sources. Such mismatching can be identified because it implies an illogical transport pathway, which crosses the longitudinal flow units of the glacier. We therefore reallocated mismatched samples to their most likely unsampled source. Specifically, debris on the west side of the glacier model-matched to Nuptse on the east was reallocated to the geologically similar Pumori source catchment, and the east side debris model-matched to Changri was reallocated to Nuptse Nup cirque, again of similar geology. There was no field evidence of supraglacial rock avalanche deposits large enough to have redistributed debris along a cross-valley axis and which could alternatively account for across-glacier transport.

**TABLE 2** Results of the Kruskal–Wallis test.

<250 $\mu\text{m}$ fraction				<2000 $\mu\text{m}$ fraction			
Element	Significance level	Mean concentration	SD	Element	Significance level	Mean concentration	SD
Al	0.013	1.8492	0.2654	Si	0.036	8.0711	0.6861
V	0.045	0.0054	0.0011	K	0.043	2.7377	0.4940
Zn	0.018	0.0080	0.0031	Ti	0.038	0.3473	0.0915
Sr	0.020	0.0147	0.0056	Mn	0.033	0.0340	0.0140
Pb	0.016	0.0036	0.0011	Fe	0.031	2.3871	0.9811
				Ni	0.021	0.0030	0.0009
				Y	0.019	0.0023	0.0010
				Zr	0.044	0.0134	0.0042
				Pb	0.014	0.0036	0.0013
				U	0.010	0.0011	0.0003
				LE	0.029	83.4043	1.4048

Note: For each grain size fraction, the table shows the combination of major element tracers, and their confidence levels, which passed the test to allow all source catchments to be distinguished from all others. Only four tracers from the <250  $\mu\text{m}$  fraction resulted in 80% discrimination, insufficient to proceed with the unmixing model.

Abbreviation: LE, light elements.

## 4.5 | Glacial debris transport model

The transport of sediment within Khumbu Glacier was simulated using a Lagrangian particle-tracking scheme implemented in a higher order ice flow model (Scherler & Egholm, 2020) based on the integrated second-order shallow ice approximation (iSOSIA) model (Egholm et al., 2011) to calculate debris (particle) transport times along englacial and supraglacial flow paths. A similar version of this glacier model was previously applied to Khumbu Glacier to simulate glacier evolution through the late Holocene (Rowan et al., 2015, 2021). The version of iSOSIA used here differs from that used in previous studies of Khumbu Glacier in that instead of treating englacial and supraglacial debris as a concentration within each cell of ice, debris transport is simulated as Lagrangian particles that are transported passively with ice flow and the particles track debris properties such as glacial transport time from the point of particle entrainment in ice flow to deposition at the ice margin. When a debris particle reaches the ice margin, it is deposited to form moraine and reworked by hillslope processes.

Rather than simulating the precise late Holocene climatic forcing and response of Khumbu Glacier, our approach broadly reproduces the change in ice mass and dynamics observed from the position of ice-marginal moraines and observations of the present-day glacier. It simulates the expected patterns of ice flow and debris transport through the LIA to about 1900 CE, prior to the onset of rapid late 20th-century mass loss and stagnation and so does not include the strongly negative trends in mass balance observed over the last 60 years (King, Bhattacharya, et al., 2020). Sediment transport based on the present-day glacier configuration would not replicate earlier states of connected tributaries and more rapid turnover. Relatively high ice levels are assumed to have persisted into the early 20th century until around 1900–1930 CE as verified by the earliest photographs of Khumbu Glacier from this period (Ward & Clark, 1992).

The experimental design follows that of Rowan et al. (2015). A spin-up glacier configuration was run for 2000 years to match the late Holocene extent (around 1.3 ka; Hornsey et al., 2022) when the glacier was assumed to be in mass balance equilibrium with the local climate. The glacier model was then forced to the present day by changing the ELA from 5478 to 5830 m a.s.l., equivalent to a change in mean annual air temperature of 1.5°C over 500 years, to represent glacier evolution from the LIA maximum (around 0.5 ka) to the present day (equivalent to 1900 CE). The model used a positive degree-day approach to simulate mass balance using an ablation constant of 2.0 mm w.e. °C<sup>-1</sup> as a function of air temperature. Air temperature at each timestep was calculated assuming a mean annual sea level air temperature of 19°C from a sinusoidal annual cycle with an amplitude of 12°C and using a lapse rate of -0.004°C km<sup>-1</sup>. Accumulation of snow on the glacier surface was simulated using a linear temperature-dependent rate and redistribution by avalanching from slopes exceeding 28°, constrained to values measured in 1974 and 1976 (Benn & Lehmkuhl, 2000; Inoue, 1977; Inoue & Yoshida, 1980). Debris was added to the glacier surface from surrounding hillslopes at a rate of 1 mm a<sup>-1</sup> in line with the estimated Holocene catchment denudation rate (Hornsey et al., 2022). Ice flow and englacial debris transport paths were simulated in three dimensions through the ice column using a 100 m × 100 m horizontal grid and 20 vertical layers. The model timestep varied with the stability of the ice flow calculation and was typically 5–6 months.

## 5 | RESULTS

### 5.1 | Multiple discriminant analysis of debris source areas

For the 250–2000 µm sediment fraction, the original 34 major elements measured in the source samples were reduced by Kruskal-Wallis analysis to 11 elements, which in combination provided the strongest statistical discrimination between source catchments (Table 2). Multiple discriminant analysis based on six sources shows a clear distinction between debris derived from these sources (Figure 4) with the model achieving 100% discrimination allowing unmixing of glacier tongue samples to be modelled with confidence. The <250 µm fraction yielded only five discriminating elements (Table 2) and so has not been further employed.

### 5.2 | Cross-glacier trends in supraglacial debris composition

Samples from transects D1–D3 were examined regarding their geochemical match to fingerprinted source areas. Results of the unmixing model for these transect samples are presented in Table 3, and an illustration of single-source contributions is in Figure 5. The D1 transect was located immediately south of the recently detached Changri Glacier confluence and includes a lithological stripe formed by dark rocks of the Western Cwm flow unit, bounded by pronounced medial moraines. This flow unit is geochemically identified by similar samples D1-5 to D1-7 within which about 50% of debris matched to the Western Cwm. At the western end of the transect, D1-8 showed a 71% match with Changri Valley sources, indicating debris in these samples was transported before the detachment of the tributary, which occurred after 1984 CE according to aerial photography. Changri Shar Glacier provided more than twice as much debris to D1-8 as Changri Nup Glacier. Towards the east, samples D1-1 to D1-3 show a strong match with Nuptse sources with a significant secondary component derived from the Lingtren–Khumbutse wall. The lack of source fingerprinting in the Nuptse Nup cirque prevents any match with that source even if debris was supplied from there. The logical barrier imposed on the model prevented debris from western sources from matching to samples from the eastern side of the glacier and debris from eastern sources from crossing to the west (see above).

The D2 transect shows a different pattern of matching from the D1 transect. Changri Valley debris comprises 45%–54% of debris within the westernmost samples D2-7 and D2-8, with Changri Shar Glacier debris again exceeding the Changri Nup Glacier contribution. These samples contain apparently significant contributions from Nuptse sources, which are likely due to model mismatching, with the former tributary of Pumori Glacier, a catchment of similar geology to Nuptse, being the likely source to which these samples are therefore reallocated. Samples D2-2, D2-3, D2-4 and D2-6 are dominated by elements derived from the Nuptse granite (Figure 5) with minor contributions from other sources. Almost no debris from the Western Cwm was identified in this transect, consistent with the disappearance of Western Cwm clast lithologies on the glacier surface below transect D1. Samples D2-2 and D2-5 are almost identical and contain significant proportions of debris matched to all

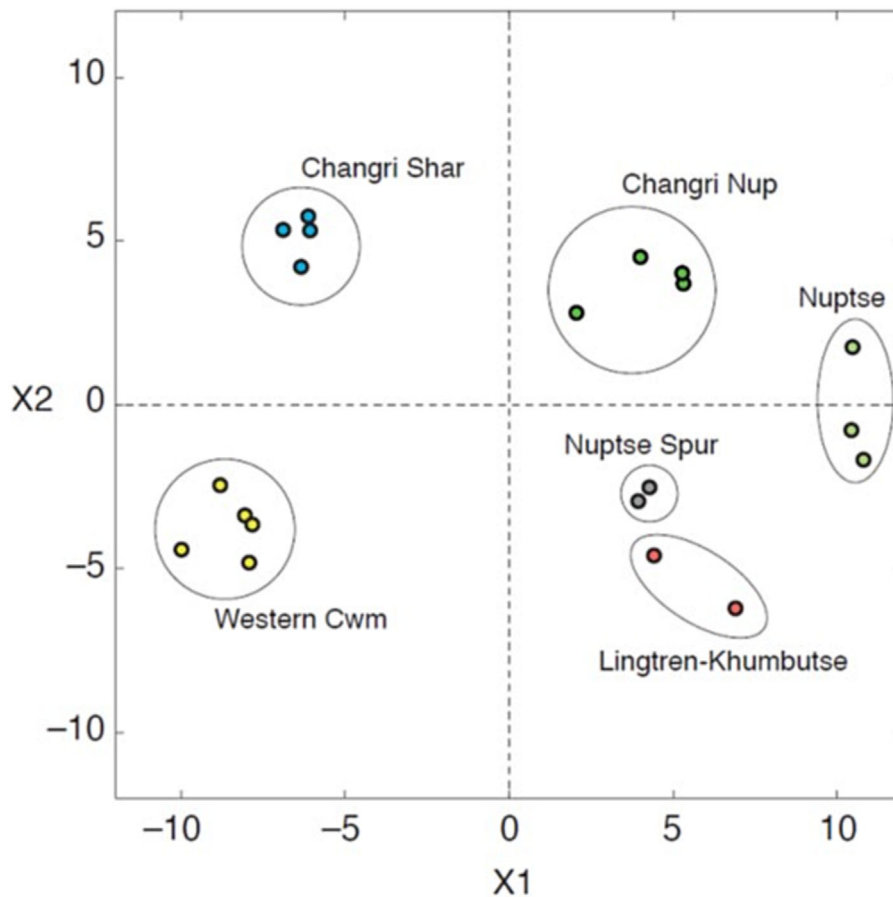


**FIGURE 4** Results of multiple discriminant analysis (MDA) of source area geochemistry. Each dot represents one sample and each cluster represents a source transect whose location is shown in Figure 1. The method effectively discriminates each source area transect from all others.

sources except the Western Cwm while differing from adjacent to Nuptse-dominated samples.

Transect D3 comprises eight samples which cluster into two similar groups. D3-1, D3-3, D3-7 and D3-8 contain 72%–93% of debris, which the model matches to eastern Nuptse sources. The model allocates 19%–34% of debris in samples D3-2, D3-4, non-conservative D3-6 and D3-8 to the Changri Valley. Lingtren–Khumbutse debris is significant in D3-4, but Western Cwm debris is almost absent. The apparent Changri Nup and Changri Shar Glacier contributions in eastern samples D3-2 to D3-5 are regarded as mismatching, and this debris was reallocated to the geologically similar Nuptse Nup cirque.

### 5.3 | Across-glacier trends in supraglacial debris composition: A three-source summary

The initial six source area discrimination was generalised into three broader groupings to highlight debris contributions from western sources (Changri Shar and Changri Nup Glaciers), eastern sources (Nuptse cirque and Nuptse spur) and Main Divide sources (the Lingtren–Khumbutse wall and the Western Cwm). Results are presented as sets of pie charts showing the relative contribution of each of these three source groupings (Figure 5). We indicate where model mismatches have been identified and reallocate these debris contributions to the most likely unsampled sources.

Debris from the Main Divide sources Lingtren–Khumbutse and (especially) the Western Cwm (Figure 5a) were concentrated in the

centre of Transect 1 but are almost absent from every other transect except in samples D1-1 and D3-5. The locations and isolation of these samples suggest that these matches may be anomalous. Physical evidence of Western Cwm debris is sparse because the lithological stripe of Everest Series clasts tapers out below the former Changri Nup Glacier confluence due to lateral compression of the Western Cwm flow unit by vigorous ice from the Nuptse cirque and, previously, from the Changri Nup Glacier. Granitic debris from eastern sources on Nuptse (Figure 5b) appears to dominate most samples, especially in the central and eastern sectors of Khumbu Glacier. Debris on the eastern side of the glacier tongue mismatched to the western Changri Valley (Figure 5c) has been reassigned to the Nuptse Nup cirque which formerly supplied mainly sillimanite gneiss. Overall, our results demonstrate a greater contribution from both western and eastern sources to mid-tongue and lower tongue transects D2 and D3 and a lesser contribution to D1 in the upper tongue.

Debris cover provenance indicates with high confidence that debris inputs from the Changri Valley were formerly relatively high but that debris from Main Divide sources has more recently become dominant as lateral tributary discharges have waned. With lower confidence, our results imply that the eastern tributaries may have supplied greater relative amounts of debris in the past but again their input has waned more recently. In the mid-tongue sector, it is demonstrated with confidence that lithological stripes disappear and that localised areas of the debris cover contain debris from mixed sources. The reasons for these patterns are discussed later.



**TABLE 3** Fractional contribution of each of the six source areas to sand samples collected on the debris-covered tongue of Khumbu Glacier.

West								East
<b>A. Transect D1: Upper tongue</b>								
Source	D1-8	D1-7	D1-6	D1-5	D1-4	D1-3	D1-2	D1-1
Nuptse cirque	0.04	0.12	0.14	0.12	0.15	<b>0.52</b>	<b>0.52</b>	<b>0.49</b>
Nuptse Spur	0.13	0.14	<b>0.24</b>	<b>0.27</b>	<b>0.78</b>	0.19	0.16	0.17
Western Cwm	0.04	<b>0.50</b>	<b>0.50</b>	<b>0.49</b>	0.02	0.00	0.00	0.13
Lingtren-Khumbutse	0.08	0.04	0.03	0.04	0.02	0.16	0.17	0.12
Changri Nup	<b>0.21</b>	0.14	0.07	0.05	0.03	0.08	0.09	0.06
Changri Shar	<b>0.50</b>	0.06	0.03	0.03	0.00	0.05	0.05	0.03
<b>B. Transect D2: Mid-tongue</b>								
Source	D2-8	D2-7	D2-6	D2-5	D2-4	D2-3	D2-2	D2-1
Nuptse cirque	0.04	0.04	0.12	0.07	0.15	0.12	0.08	0.17
Nuptse Spur	0.34	<b>0.23</b>	<b>0.73</b>	<b>0.54</b>	<b>0.74</b>	<b>0.73</b>	<b>0.52</b>	0.01
Western Cwm	0.06	0.08	0.00	0.00	0.01	0.00	0.00	0.00
Lingtren-Kumbutse	0.10	0.10	0.04	0.11	0.02	0.04	0.11	0.00
Changri Nup	0.12	0.17	0.08	0.18	0.06	0.08	0.19	<b>0.77</b>
Changri Shar	<b>0.33</b>	<b>0.37</b>	0.03	0.10	0.02	0.03	0.10	0.04
<b>C. Transect D3: Lower tongue</b>								
Source	D3-8	D3-7	D3-6	D3-5	D3-4	D3-3	D3-2	D3-1
Nuptse cirque	0.09	0.15	0.09	0.08	<b>0.29</b>	0.11	0.04	0.11
Nuptse Spur	<b>0.63</b>	<b>0.78</b>	<b>0.56</b>	<b>0.45</b>	<b>0.21</b>	<b>0.77</b>	<b>0.48</b>	<b>0.75</b>
Western Cwm	0.00	0.03	0.02	0.14	0.05	0.00	0.04	0.00
Lingtren-Khumbutse	0.08	0.02	0.10	0.07	<b>0.21</b>	0.05	0.10	0.05
Changri Nup	0.13	0.01	0.17	0.11	0.05	0.04	0.07	0.05
Changri Shar	0.06	0.00	0.07	0.15	<b>0.20</b>	0.03	<b>0.27</b>	0.03

Note: Bold type highlights source contributions  $\geq 0.20$ . A–C are arranged in a north-to-south (downglacier) direction.

## 5.4 | Glacier model simulations of particle transport

The glacier model calculated the time elapsed for particles to be transported from the location of their initial entrainment (hereafter, debris age in years). The model also calculated the integrated particle transport time represented by each englacial flowline that terminated within the present-day supraglacial debris layer. The debris age exceeded the flowline time where particle transport was interrupted by deposition and re-entrainment of debris. Although the flowline time was relatively consistent across glaciers, representing the duration of longitudinal ice flow, the debris age was more variable, representing the processes that transport debris from tributary catchments to the main glacier tongue (Figure 6).

Debris transport through the tongue of Khumbu Glacier was calculated by comparing the flowline time for each particle relative to two ‘flowgates’ representing the upper and middle sections of the ablation area, one at the base of the Khumbu Icefall and another upglacier of the Changri Nup confluence close to Gorak Shep Village (Figure 1). The flowline time from upglacier of the Icefall flowgate was  $132 \pm 0$  years and to the Gorak Shep flowgate was  $369 \pm 5$  years. The flowline time sampled from each of the tongue transects D1–D3 increased with distance downglacier (Figure 6, Table 4) from 275 years through source transect S3 to 395 years at transect D1, 485 years at D2 and 520 years at D3. It should be noted that the

flowline time captures the movement of particles through the vertical ice column and will therefore be longer than the time represented by the equivalent horizontal displacement that could be measured at the glacier surface (cf. Quincey et al., 2009). Supraglacial particle age (Table 4) in the source transects indicates the duration of transport, including periods of deposition and re-entrainment before the debris was incorporated into the main tongue of Khumbu Glacier. Supraglacial particles are generally not present at source transects located close to the LIA ELAs because debris here was in englacial transport. The few debris particles found at the surface of the source transects in the LIA simulations give ages between 1600 and 1900 years.

Particle age in the tongue transects indicates the duration of transport, including periods of deposition and re-entrainment in the main tongue of Khumbu Glacier. For transect D1, particle age across the glacier averaged  $1150 \pm 667$  years where the oldest ages were located at the ends of the transect. Both transects D2 and D3 show particle ages, which differ across the glacier tongue. At D2, points on the true left side of the glacier had ages of  $509 \pm 0$  years, and those on the true right had ages of  $924 \pm 0$  years. At D3, the mean debris age was  $788 \pm 194$  years with older debris in the centre of the glacier ( $1007 \pm 0$  years) and younger debris in the centre-right of the glacier ( $616 \pm 69$  years). These cross-glacier particle age differences are caused by the different transport times through source catchments before tributary glaciers joined the main glacier tongue (Figure 6).

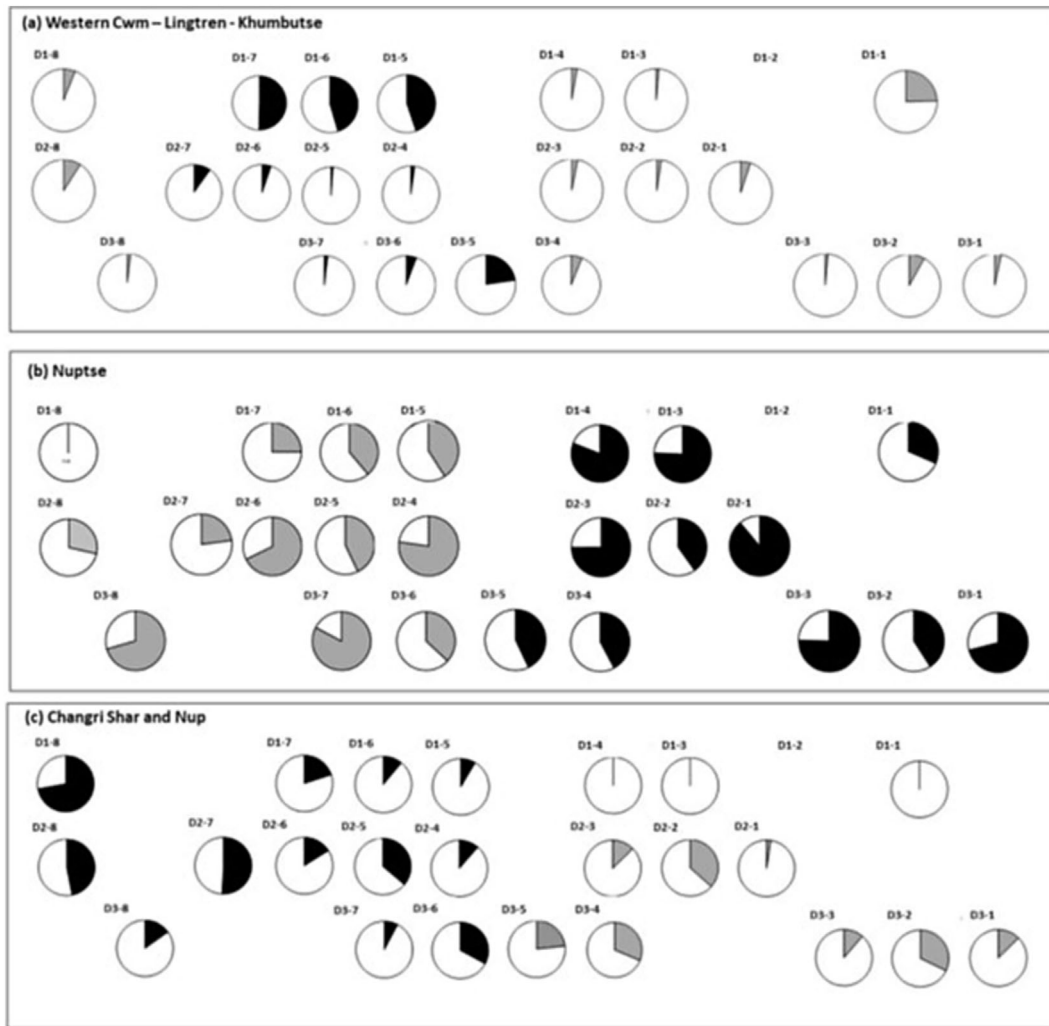


**FIGURE 5** Graphical representation of the debris contribution from each of the three main sources as measured by the unmixing model. Panel (a) combines the Main Divide sources of the Western Cwm and the Lingtren–Khumbutse wall (transect S3), panel (b) combines Nuptse spur and Nuptse cirque (transect S4) and panel (c) combines Changri Nup and Changri Shar glaciers (transects S1 and S2). In each panel, the upper, middle and lower rows represent debris tongue transects D1, D2 and D3, respectively, and samples are numbered from right (east) to left (west). Black fills represent source allocations accepted from the model, and grey fills represent contributions allocated by the model to the named source but manually reallocated on a common sense (see text).

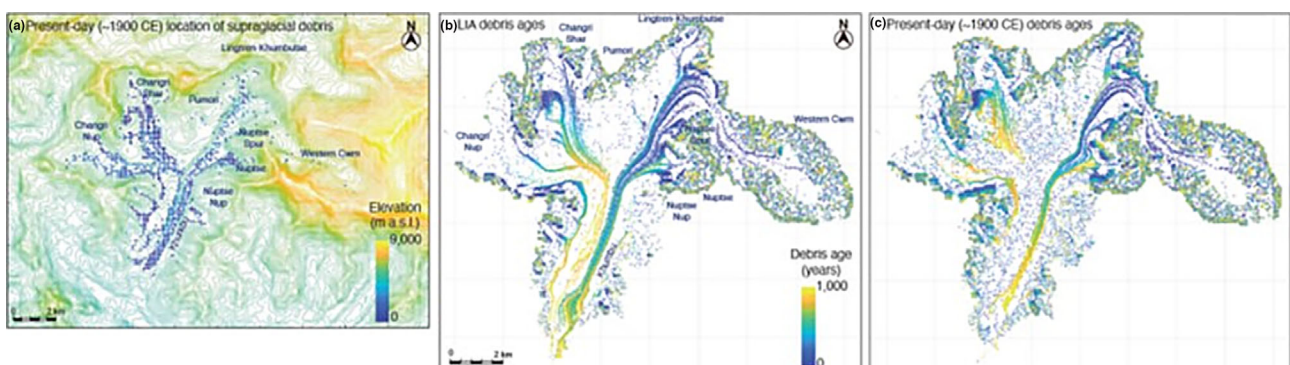


**FIGURE 6** Results from the particle-tracking model showing (a) the location of supraglacial debris particles in the present-day (c. 1900 CE) simulation. Simulated debris ages and glacial flowlines are shown for (b) the Little Ice Age (LIA) glacier configuration and (c) the present-day (c. 1900 CE) glacier configuration. The colour scale for debris age represents the time in years that the debris particle has been in transport since initial erosion from the surrounding hillslopes. Where particles are shown outside the glacier on the surrounding hillslopes, the particle age represents the duration of non-glacial sediment transport, for example, by mass wasting or through ice-marginal moraines.

**TABLE 4** Results from the glacier model giving the time in years represented by flowlines from the accumulation area in the Western Cwm to transects in the ablation area of the glacier tongue, along with the age of supraglacial debris at each transect from the Little Ice Age simulation.

A. Little Ice Age simulation				
Transect	Flowline time from source (years)	Flowline time difference from nearest upglacier transect (years)	Debris age range across transect (years)	Mean transect debris age (years)
S3	273 ± 5	273	-	-
D1	393 ± 3	120	427–1878	1150 ± 667
D2	483 ± 2	90	509–924	758 ± 227
D3	521 ± 0	38	836–1411	1045 ± 318
B. Present-day simulation				
Transect	Flowline time from source (years)	Flowline time difference from nearest upglacier transect (years)	Debris age range across transect (years)	Mean transect debris age (years)
S3	296 ± 8	296	-	-
D1	517 ± 7	221	734–2180	1411 ± 662
D2	949 ± 24	432	565–2371	1311 ± 669
D3	0	-	527–1007	788 ± 194

Note: Values representing each transect are given as the mean and standard deviation. Note that supraglacial debris is not present in the simulated source transect. In the results for the present-day simulation, the flowline time is 0 at the transect closest to the glacier terminus (D3) as the present-day terminus has receded from the location of this transect to leave the ice-cored moraine. Results from the little ice age simulation are shown in (a) and from the present-day simulation for comparison in (b).

## 6 | DISCUSSION

### 6.1 | Limitations of the sediment unmixing model

The FR2000 sediment unmixing model has not previously been used in glacial environments and was successful in tracing the provenance of supraglacial debris on Khumbu Glacier. The number and distribution of samples collected from source catchments discriminate effectively between sources based on 11 major elements within the 250–2000 µm grain size fraction. However, the unmixing model requires both a clear geochemical distinction of source areas and a distribution of source and debris tongue samples to capture debris from all potential contributing sub-catchments. Failure to satisfy the second criterion resulted in portions of debris samples being matched to the wrong source area. This problem was mitigated by the manual reallocation of mismatched debris components, based on the assumption that laminar ice flow within a valley precludes source and debris samples from being located on opposite sides of the glacier. Pumori Glacier and Nuptse Nup cirque could not be accessed during the field campaign, so the model tends to mismatch debris from these sources to the geochemically most-similar fingerprinted sources, that is, Pumori Glacier to Nuptse and Nuptse Nup cirque to Changri Nup Glacier.

Non-conservative behaviour (Section 3.3) was observed in three debris samples: in sample D3-6 all elements except Mn, Ni and U exhibited non-conservative behaviour; sample D2-2 showed non-conservative behaviour of K and Pb; and sample D1-2 showed Pb was non-conservative. These samples were retained in our interpretation because most elements lay within the range of source samples but some caution is needed in their interpretation. Non-conservatism could be reduced by taking a greater number of source samples to capture the entire range of lithological variation within the contributing tributary catchments.

### 6.2 | Limitations of the particle transport model

Net glacier mass balance drives the rate of mass flux (ice flow) through a glacier and therefore affects the distribution of ages of englacial debris. The debris and ice ages simulated using iSOSIA are sensitive to the choice of mass balance variables used to force the glacier model, which is a complex uncertainty to estimate as the mass balance is transient and a function of the evolving debris layer. Our previous studies demonstrated that the iSOSIA experimental design used here accurately represents the evolution of Khumbu Glacier through the late Holocene (1.3 ka to present) as indicated by geomorphological evidence of glacier extent and remote sensing observations of recent glacier volume change and velocities. The mass balance sensitivity of the glacier model between the LIA and the present day was assessed, and the simulated velocities were evaluated against observations in Rowan et al. (2015), and a rigorous assessment of the sensitivity of glacier mass change and velocity to mass balance forcing between 1984 and 2015 CE was undertaken in Rowan et al. (2021). These results showed that the simulated rate of ice flow (and hence ice and debris ages) did not vary dramatically between consecutive decades for different mass balance parameterisations even when changes in ice mass occurred (Rowan et al., 2021). We therefore consider that the simulated debris and ice ages reliably indicate these values for the period of several decades around the specified period and that uncertainties in the choice of mass balance variables do not significantly influence our results. The debris-covered tongue of Khumbu Glacier dynamically detached from the upper active glacier in the early 20th century (Rowan et al., 2021) and, as a result, the age of the ice downglacier of the Gorak Shep flowgate is unlikely to be influenced by recent changes in glacier mass balance, which motivated our choice of 1900 CE to represent the most recent dynamic configuration of the entire Khumbu Glacier.

The glacier model grid spacing was  $100 \times 100$  m and the results indicate the simulated values at this resolution rather than precisely matched to the point sampling of debris provenance. However, the spacing of sampling points across all the transects is sufficiently well-spaced to be compared with the model outputs. Khumbu Glacier extended past the location of transect D3 during the LIA but not during the present-day simulation, reflecting the observed recession of the terminus of 1.5 km during this period (Rowan et al., 2021). The debris layer at this point therefore represents the upper surface of an ice-cored moraine that is a remnant of the LIA tongue of Khumbu Glacier.

### 6.3 | Geochemical patterns due to lateral variation in ice discharge

Our results show a downstream evolution of the geochemical composition of the Khumbu Glacier debris cover in which coherent compositional striping at transect D1, verified by field observations of clast lithology, becomes imperceptible in the mid-tongue where it is replaced by the dominance of elements derived from the tributary catchments of Changri Nup, Changri Shar and Pumori glaciers to the west and Nuptse to the east. However, samples of mixed composition increased in number downstream from two in transect D2 to four in transect D1. This spatial pattern of debris provenance shows clear evidence of changes in the contributions of tributary glaciers to the main Khumbu Glacier, with increasing secondary reworking towards the terminus.

In the upper glacier tongue (transect D1), Main Divide sources dominate the central and western portion of the debris cover with most debris derived from the Western Cwm via the Khumbu Icefall. Relatively minor Lingtren–Khumbutse debris supply reflects lower glacier discharge from these hillslopes, and this source is only significant in the westernmost debris sample (D1-8). Nuptse debris dominates the east side of the debris cover.

The mid-glacier tongue (transect D2) has a surprising lack of Western Cwm debris but greater contributions from the Changri Valley western tributaries. Western samples contain persistent minor contributions from the Lingtren–Khumbutse sourced debris and debris possibly derived from the now-detached Nuptse Nup cirque in samples near the eastern glacier margin. Granitic Nuptse debris dominates the central and eastern parts of the debris cover. The lack of Western Cwm debris downstream of transect D1 is tantalising. Field observation shows rapid physical disintegration of Everest Series lithologies, although residual chemical elements should reside in the debris cover and might be expected in mid-glacier samples (D2-4 to D2-6). Fine debris released by clast weathering is unlikely to have been entirely eluviated and removed. We therefore suggest that our sampling has missed this flow unit at transect D2, perhaps because Western Cwm ice is laterally compressed to the extent it becomes narrow enough to fall between our spaced samples. Furthermore, debris discharge from the Western Cwm is relatively low. The Khumbu Icefall represents the least debris-covered tributary to Khumbu Glacier despite the high rate of ice flow (Altena & Käab, 2020). Ice-covered slopes above 6000 m are likely cold based and probably non-erosive. Debris is derived from these ice-free slopes by gravitational processes (Scherler, 2014) particularly the

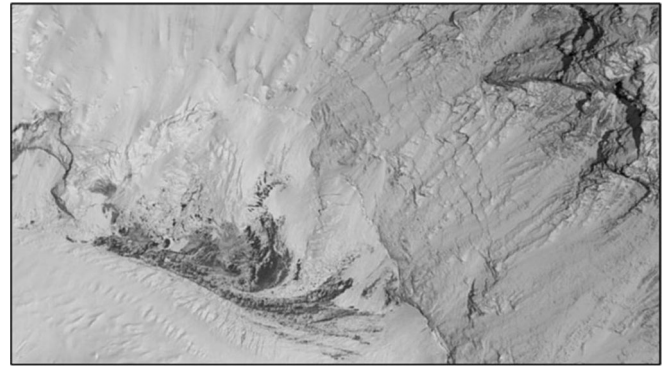


**FIGURE 7** Aerial image of part of the Western Cwm and base of the south-west face of Mt. Everest (Sagarmatha). Trails of rockfall-derived supraglacial debris occur around 6400 m elevation, derived from rock falls. In pre-monsoon conditions, the face is largely bare rock and becomes snow-covered in the post-monsoon period. This debris stream was sampled down-flow below the Khumbu Icefall in source transect 3. The image is  $\sim 2$  km across at the base and the location is indicated in Figure 1 (Google Earth™ image, 2017).

2000-m-high ice-free south-west face of Sagarmatha where abundant supraglacial rockfall debris is visible on the glacier surface (Figure 7). The debris is constrained to a very narrow flow path along the true right side of the Western Cwm flow unit, with ‘clean’ ice from the hillslopes of Lhotse and Nuptse making up most of the flow unit.

In the lower glacier tongue (transect D3), the major component in the western portion probably originated from the granitic source of Pumori Glacier (D3-7 and D3-8; mismatched to Nuptse). The eastern part of the tongue (D3-1 to D3-3) clearly originated from the Nuptse catchment. Four samples have mixed sources without a dominant source component. Three of these (D3-4, D3-5 and non-conservative D3-6) were collected in the centre of the glacier and one (D3-2) to the east. These mixed samples cannot rationally be explained by tributary variations and are explained as evidence of secondary reworking. Significant Main Divide debris occurs in the glacier centre and in lesser amounts in other mixed samples in the transect, indicating that a narrow ice flow unit from this source did reach the glacier terminus during the LIA as indicated by the particle-tracking glacier model (Figure 6).

### 6.4 | Glacier structures influenced by changing tributary discharges

Our sample spacing was not sufficiently dense to compile a precise map of debris provenance across the entire debris-covered tongue. However, the evidence is sufficient to infer how changing tributary discharges determined patterns of supraglacial debris composition across the compound glacier tongue. The hypothetical model of debris cover evolution has two basic states where the sources of ice flowing through Khumbu Glacier are either tributary-dominated or Main Divide-dominated (Figure 8). The relief and proximity of the Nuptse cirque means that ice from this source was always confluent under both states. In both states, ice flow units form parallel flowlines within a compound tongue with a simple longitudinal structure. A state of

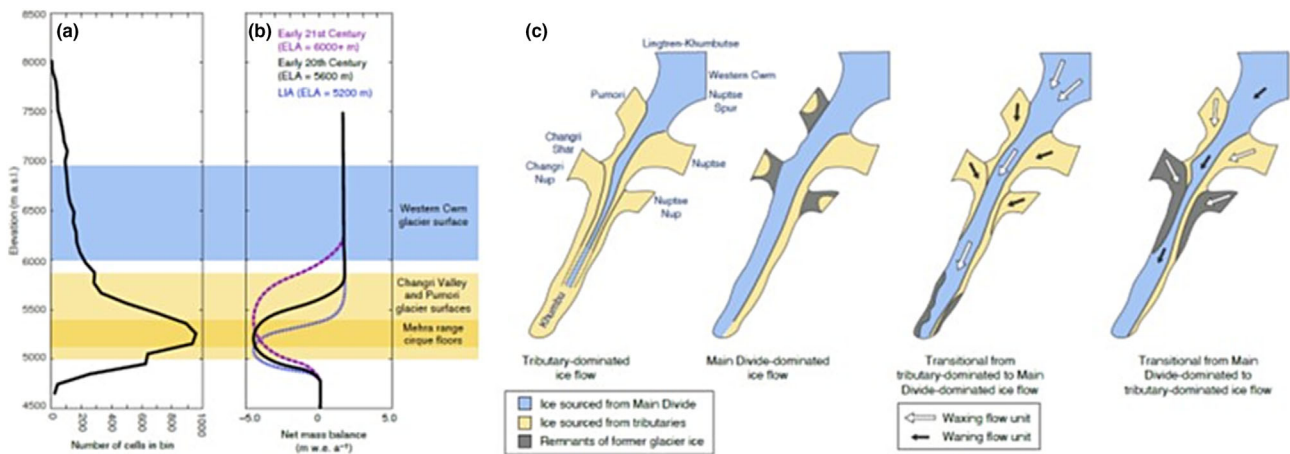


**FIGURE 8** The impact of change in equilibrium line altitude (ELA) on ice flow and debris transport through Khumbu Glacier. The altitudinal range of glacier surfaces for tributary catchments in relation to (a) the catchment hypsometry and (b) the vertical mass balance profile. The early 20th-century mass balance profile is after Inoue (1977) and is illustrated to represent the Little Ice Age ELA and early 21st-century ELA using values produced from simulations of the evolution of the Khumbu Glacier through the late Holocene (Rowan et al., 2015). Note the coincidence of temporal shifts in the mass balance profile with the elevation of the glacier surfaces and cirque floors for the Changri Valley, Pumori and Mehra glaciers. (c) Schematic illustration of the different dynamic states of the structure of the glacier tongue due to changes in the importance of flow units sourced from different tributaries. The current geochemical pattern in the debris cover implies the glacier is currently in transition from a tributary-dominated to a Main Divide-dominated state.

tributary dominance prevailed when the mass balance in the eastern and western tributary catchments was more strongly positive than the mass balance in the Main Divide zone (Figure 8a). Vigorous ice flux from the tributaries nourished flow units occupying a greater proportion of the glacier tongue's width and even weaker tributaries which ablated away at upstream termini added supraglacial debris to Khumbu Glacier. Ice from the Main Divide formed a narrow medial ice flow unit which may not have reached the compound glacier terminus. Conversely, a state of Main Divide dominance prevailed when the mass balance is more strongly positive in the Main Divide catchments, particularly the Western Cwm (Figure 8b). In this state, weaker tributaries may have detached from the main tongue or have low rates of ice and debris flux, whereas ice flow from the Western Cwm and Lingtren-Khumbutse sources occupied most (or, if other tributaries detached, all) of the width of Khumbu Glacier. Complexity arises during the transition between dynamic states; a transition from tributary-dominated to Main Divide-dominated ice flow resulted in tributary flow units that were restricted to narrow marginal zones or detached as their discharges waned (Figure 8c). Our results demonstrate that ice from the Main Divide reached the lower glacier tongue, and therefore, remnants of debris-covered tributary glaciers may be preserved in marginal locations near the terminus. Debris from Changri Nup and Changri Shar Glaciers and the eastern tributary catchments was incorporated as discrete zones within the Khumbu Glacier tongue. A transition from Main Divide-dominated to tributary-dominated ice flow (Figure 8d) resulted in the narrowing of the Main Divide ice flow units as tributary discharges increased, whereas Main Divide ice occupied the lower portion of the tongue before being replaced by tributary ice flow.

Our results indicate that Khumbu Glacier has undergone a transition from tributary-dominated to Main Divide-dominated ice flow in recent decades as the tributaries have waned and detached. This change occurred during a period of generally negative mass balance so that ice flow from the Main Divide became more important

because the sources had higher elevations and therefore less negative mass balance than the lower elevation tributary glaciers under a warming climate. Field evidence supports this interpretation; supraglacial debris close to Gorak Shep is granitic against the right-lateral moraine face, which is composed largely of sillimanite gneiss. Thus, the ice flow unit that deposited the lateral moraine was different from the ice flow unit currently in contact with the moraine. The negative trajectory of change will eventually lead to the physical detachment of the lower debris-covered tongue of Khumbu Glacier from the upper active glacier flowing from the Main Divide source areas (Naito et al., 2000; Rowan et al., 2021). Simulation of debris flowline ages using the particle-tracking glacier model allowed a timescale to be placed on the transition of Khumbu Glacier between a state of tributary-dominated to a state of Main Divide-dominated ice flow. The mean flowline time to transect D1 is about 390 years and to D2 is about 480 years suggesting that the transition began within the last 400 years and that tributary dominance prevailed for at least several centuries beforehand (Figure 6). The present glacier tongue comprises ice that accumulated and flowed downglacier within the last 500 years. The exception is the terminal zone below D3 where simulated flowline ages exceed 520 years. Here, ice structures appear complex and convoluted, indicative of a long and possibly complex strain history, and the very thick debris cover contains abundant rounded, sorted and comminuted material including much non-granitic debris (Fushimi, 1977).

## 6.5 | Reworking of debris by secondary processes

The coherent pattern of source contributions to the upper glacier tongue at transect D1 diffused downglacier. The mid-tongue sector had two mixed-source samples (D2-2 and D2-5) compared to the lower tongue transect D3 where there were four mixed-sources samples; three of which (D3-4 to D3-6) were located near the glacier

centre. The compositional make-up of these samples cannot be explained by the structural processes outlined above, because ice flow units from different tributaries conserve the heterogeneity of their contributing debris. These samples indicate the local homogenisation of debris from different sources within the debris cover by one or more secondary processes. Local downslope mass movements are associated with relief formation and inversion and can move sediment across-glacier over length scales of tens to hundreds of metres on long medial moraine slopes (e.g., Mölg et al., 2020; Moore, 2018, 2021; Westoby et al., 2020; Bartlett et al., 2021; [Supplementary Material](#)). Entrainment and redeposition by seasonal englacial and supraglacial streamflow, along with rare outburst floods, will also transport significant debris loads in a range of directions across the glacier surface (Miles et al., 2018, 2019).

To adequately interpret the role and distribution of supraglacial debris reworking, our results are compared to Iwata et al.'s (1980) geomorphological zoning of the debris cover and aerial photography from 1984 and 2019 (Figure 3). The present-day glacier surface shows wide areas of chaotic ablation topography with steep ice and debris slopes, ephemeral ponds and stream channels (Bartlett et al., 2021; King, Turner, et al., 2020). In contrast, an extensive area of stable darker debris occurs along the lower west margin of the tongue, widening to encompass the full glacier width above the terminus. The stable zone shows a relatively high elevation and low relief compared to neighbouring chaotic topography, with nascent soil development and vegetation colonisation, and its few ponds have relatively low turbidity. It is truncated along its eastern edge by a debris-covered ice slope. Fluvial activity is focused along the east side of the glacier below this slope, where streams link a chain of large ponds along a longitudinal valley (Miles et al., 2019). This sector has developed since aerial photographs taken in 1984 when the principal meltwater drainage occurred englacially (Figure 3). Subsequently, the former englacial stream has emerged as a supraglacial system as the glacier has thinned towards the hydraulic grade line of the englacial drainage (cf. Kirkbride, 1993). The glacier surface in this sector lowered by 40–70 m between 1962 and 2018 (King, Bhattacharya, et al., 2020). Chaotic topography is associated with local melt centres where debris cover of locally variable thickness promotes enhanced differential ablation and relief creation with ice cliff formation by supraglacial streams and ponds (King, Turner, et al., 2020).

## 6.6 | Climatic drivers of glacier change

Khumbu Glacier characterises the vertical mass balance gradient of high-elevation monsoon-influenced glaciers (Benn & Lehmkuhl, 2000). The ELA is located within the icefall, with a low positive mass balance above the late-20th-century ELA at around 5600 m a.s.l. (Inoue, 1977) that has risen to approximately 6000–6400 m a.s.l. during the early 21st century (Rowan et al., 2015, 2021) due primarily to atmospheric warming (Kayastha & Harrison, 2008; Thakuri et al., 2014). Below the ELA, negative balance increases in a narrow altitudinal range as the debris cover thickens and generally reduces melting towards the terminus (Figure 8), although extensive differential ablation in recent decades has led to increased sub-debris melt across the entire ablation area (Rowan et al., 2021). Above the ELA, accumulation is strongly influenced by snow avalanching and is

insensitive to altitude (Benn & Lehmkuhl, 2000). The upper slopes of Sagarmatha remain largely snow-free in the pre-monsoon season due to low winter precipitation and extreme wind speeds close to the tropopause (Khadka et al., 2021). The mass balance gradient is highly relevant to why the structure of the lower glacier alters between tributary-dominated and Main Divide-dominated ice flow (Figure 8). The mass balance of the Western Cwm, whose floor lies above 6000 m a.s.l. and surrounding ridges range from 7600–8848 m a.s.l., was largely insensitive to the past centennial range of ELA variations (Rowan et al., 2021). In contrast, the lateral tributaries of Khumbu Glacier (Changri Nup, Changri Shar and Pumori glaciers and Nuptse Nup cirque) have surfaces in the range 5200–5800 m a.s.l., and their mass balances were sensitive to post-LIA variations in ELA. Changes in glacier structure indicated by debris provenance were driven primarily by variations in mass balance in the lower altitude tributary valleys. Mass balance changes in the central and eastern Himalaya are generally understood to be driven primarily by variations in monsoon strength (Finkel et al., 2003; Murari et al., 2014; Owen et al., 2005; Owen et al., 2009) with which the Holocene moraine chronology of Khumbu Glacier is consistent (Hornsey et al., 2022).

Our results demonstrate that the Western Cwm flow unit was the dominant source of ice to Khumbu Glacier since around 1600 CE and that relatively greater ice discharges from tributary sources reached the glacier tongue until around 1500 CE. The timing of this transition could be attributed to the weakening of the South-East Asian Monsoon at 1420 CE (Kaspari et al., 2007; Rowan, 2017). A stronger pre-1420 CE monsoon associated with lower ELAs would have allowed greater relative tributary discharges, providing the debris in transects D2 and D3 which the unmixing model matches to the eastern and western tributaries. A weaker LIA monsoon combined with lower mean annual air temperatures (Rupper et al., 2009) allowed a greater relative ice discharge from the Western Cwm to be established in the following decades. However, LIA glacier thickening did not reach the levels achieved before the LIA, instead peaking at the height of the main lateral moraine of Khumbu Glacier dated to  $1.3 \pm 0.1$  ka (Hornsey et al., 2022).

## 7 | CONCLUSIONS

We combined a sediment source unmixing model and a particle-tracking ice flow model to identify variations in the provenance of the supraglacial debris layer on Khumbu Glacier, Nepal Himalaya, as a record of dynamic glacier change in response to late Holocene climate change. The FR2000 sediment unmixing model discriminated between source catchments and matched glacier tongue samples to geochemically fingerprinted source areas. Unsampled sources led to model mismatching of some debris samples which was corrected by manual adjustment using a common-sense understanding of the glacier flow structure and could be improved by collection of the greater number of samples from each transect. The supraglacial debris layer on Khumbu Glacier contains a centennial archive of past glacier change in a geochemical pattern, which indicates changes in the contribution of tributary glaciers to the main glacier tongue. The relative timing of change can be inferred from the distance that ice has flowed while transporting debris from the glacier headwalls. The recent importance of ice flowing from the Main Divide including the Western Cwm with

minor contributions from the eastern and western tributary glaciers was not a constant feature of Khumbu Glacier's flow regime. In the past, relatively less ice and debris were derived from the Main Divide and relatively more from the Changri Nup and Changri Shar and Pumori Glacier tributaries to the west, with a lesser but significant input from Nuptse Nup cirque to the east. These changes in tributary ice supply are modulated by mass balance perturbations reflected by equilibrium line altitude changes from around 5400 m a.s.l. to above 6000 m a.s.l., which sensitise the lower altitude tributaries to ice discharge variations while scarcely affecting the extremely high-elevation Western Cwm glacier.

Application of a particle-tracking ice flow model to simulate glacier evolution through the late Holocene constrained the timing of the transition from tributary-dominated to Main Divide-dominated ice flow by calculating flowline ages representing the time elapsed between ice formation and its arrival at the transect locations on the main glacier tongue. Simulated flowline ages indicated greater ice discharge from eastern and western tributary glaciers during a period with a stronger monsoon before 1420 CE, with Main Divide-dominated ice flow becoming established in the last 400 years of colder LIA temperatures.

This novel methodology is suitable for provenance studies at other debris-covered compound valley glaciers where the necessary sampling requirements are met. It is not necessary to have detailed geological information if contributing tributary glaciers can be accessed to sample source areas close to their junctions with the main tongue. Major-element geochemistry is also shown to distinguish debris derived from lithologically similar source catchments. Further development of this work might include collecting a greater density of samples across a debris-covered glacier tongue, to better understand the reworking processes which contribute to debris cover formation and stability and which may redistribute the contained cosmogenic isotope inventory from which catchment denudation calculations can be derived.

## ACKNOWLEDGEMENTS

MPK acknowledges the support of the Mount Everest Foundation and the Quaternary Research Association. AVR was supported by a Royal Society Dorothy Hodgkin Research Fellowship (DHF/R1/201113). Fieldwork was supported by the 'EverDrill' NERC Grant awarded to the Universities of Leeds and Sheffield (NE/P00265X) and Aberystwyth University (NE/P002021). The authors thank Himalayan Research Expeditions, Kathmandu, for their support and guidance during fieldwork. All sediment samples were collected with the permission of the Sagarmatha National Park authority and exported from Nepal with the permission of the Government of Nepal through the Department of National Parks and Wildlife Conservation. We acknowledge the constructive comments of two anonymous reviewers.

## DATA AVAILABILITY STATEMENT

The geochemical dataset can be accessed at <https://zenodo.org/badge/DOI/10.5281/zenodo.7389859.svg>

The particle-tracking version of iSOSIA is available through Scherler, D. and Egholm, D.L. (2020) Chhota Shigri Glacier simulations and cosmogenic nuclide data. GFZ Data Services. [10.5880/GFZ.3.3.2020.004](https://doi.org/10.5880/GFZ.3.3.2020.004)

## ORCID

Martin P. Kirkbride [ORCID](https://orcid.org/0000-0002-7108-4382) <https://orcid.org/0000-0002-7108-4382>  
 Ann V. Rowan [ORCID](https://orcid.org/0000-0002-3715-5554) <https://orcid.org/0000-0002-3715-5554>  
 Duncan J. Quincey [ORCID](https://orcid.org/0000-0002-7602-7926) <https://orcid.org/0000-0002-7602-7926>  
 Bryn Hubbard [ORCID](https://orcid.org/0000-0002-3565-3875) <https://orcid.org/0000-0002-3565-3875>  
 Katie Miles [ORCID](https://orcid.org/0000-0003-2793-9766) <https://orcid.org/0000-0003-2793-9766>

## REFERENCES

- Altena, B. & Käab, A. (2020) Ensemble matching of repeat satellite images applied to measure fast-changing ice flow, verified with mountain climber trajectories on Khumbu icefall, Mount Everest. *Journal of Glaciology*, 66(260), 905–915. Available from: <https://doi.org/10.1017/jog.2020.66>
- Anderson, R.S. (2000) A model of ablation-dominated medial moraines and the generation of debris-mantled glacier snouts. *Journal of Glaciology*, 46(154), 459–469. Available from: <https://doi.org/10.3189/172756500781833025>
- Bartlett, O.T., Ng, F.S.L. & Rowan, A.V. (2021) Morphology and evolution of supraglacial hummocks on debris-covered Himalayan glaciers. *Earth Surface Processes and Landforms*, 46(3), 525–539. Available from: <https://doi.org/10.1002/esp.5043>
- Benn, D.I., Bolch, T., Hands, K., Gulley, J., Luckman, A., Nicholson, L.I., et al. (2012) Response of debris-covered glaciers in the Mount Everest region to recent warming, and implications for outburst flood hazards. *Earth-Science Reviews*, 114(1–2), 156–174. Available from: <https://doi.org/10.1016/j.earscirev.2012.03.008>
- Benn, D.I. & Lehmkuhl, F. (2000) Mass balance and equilibrium-line altitudes of glaciers in high-mountain environments. *Quaternary International*, 65–66, 15–29. Available from: [https://doi.org/10.1016/S1040-6182\(99\)00034-8](https://doi.org/10.1016/S1040-6182(99)00034-8)
- Bolch, T., Buchroithner, M., Peters, J., Baessler, M. & Bajracharya, S. (2008) Identification of glacier motion and potential dangerous lakes in the Mt Everest region/Nepal using spaceborne imagery. *Natural Hazards and Earth System Sciences*, 8(6), 1329–1340. Available from: <https://doi.org/10.5194/nhess-8-1329-2008>
- Bolch, T., Buchroithner, M., Pieczonka, T. & Kunert, A. (2008) Planimetric and volumetric glacier changes in the Khumbu Himal, Nepal, since 1962 using Corona, Landsat TM and ASTER data. *Journal of Glaciology*, 54(187), 592–600. Available from: <https://doi.org/10.3189/002214308786570782>
- Bolch, T., Pieczonka, T. & Benn, D.I. (2011) Multi-decadal mass loss of glaciers in the Everest area (Nepal Himalaya) derived from stereo imagery. *The Cryosphere*, 5(2), 349–358. Available from: <https://doi.org/10.5194/tc-5-349-2011>
- DiLabio, R.N.W. & Shilts, W.W. (1978) Compositional variation of debris in glaciers, Bylot Island, district of Franklin. *Current Research, Part B, Geological Survey of Canada*, Paper 78-1B, 91–94. <https://emrlibrary.gov.yk.ca/gsc/papers/78-1B.pdf>
- Egholm, D.L., Knudsen, M.F., Clark, C.D. & Lesemann, J.E. (2011) Modeling the flow of glaciers in steep terrain: the integrated second-order shallow ice approximation (iSOSIA). *Journal of Geophysical Research*, 116(F2), F02012. Available from: <https://doi.org/10.1029/2010JF001900>
- Finkel, R.C., Owen, L.A., Barnard, P.L. & Caffee, M.W. (2003) Beryllium-10 dating of Mount Everest moraines indicates a strong monsoon influence and glacial synchronicity throughout the Himalaya. *Geology*, 31(6), 561–564. Available from: [https://doi.org/10.1130/0091-7613\(2003\)031%3C0561:BDOMEM%3E2.0.CO;2](https://doi.org/10.1130/0091-7613(2003)031%3C0561:BDOMEM%3E2.0.CO;2)
- Franks, S.W. & Rowan, J.S. (2000) Multi-parameter fingerprinting of sediment sources: uncertainty estimation and tracer selection. In: Bentley, I.R., Sykes, J.F., Gray, W.G., Brebbia, C.A. & Pinder, G.F. (Eds.) *Computational methods in water resources XIII*. Rotterdam: Balkema.
- Fushimi, H. (1977) Structural studies of glaciers in the Khumbu region. *Seppyo*, 39, 30–39. Japanese Journal of Snow and Ice Special Issue.
- Hambrey, M.J., Quincey, D.J., Glasser, N.F., Reynolds, J.M., Richardson, S.J. & Clemmens, S. (2008) Sedimentological, geomorphological and dynamic context of debris-mantled glaciers, Mount

- Everest (Sagarmatha) region, Nepal. *Quaternary Science Reviews*, 27(25–26), 2361–2389. Available from: <https://doi.org/10.1016/j.quascirev.2008.08.010>
- Haritashya, U.K., Pleasants, M.S. & Copland, L. (2015) Assessment of the evolution in velocity of two debris-covered valley glaciers in Nepal and New Zealand. *Geografiska Annaler*, 97A(4), 737–751. Available from: <https://doi.org/10.1111/geoa.12112>
- Herreid, S. & Pellicciotti, F. (2020) The state of rock debris covering Earth's glaciers. *Nature Geoscience*, 13(9), 621–627. Available from: <https://doi.org/10.1038/s41561-020-0615-0>
- Hornsey, J., Rowan, A.V., Kirkbride, M.P., Livingstone, S., Fabel, D., Rodes, A., et al. (2022) Be-10 dating of ice-marginal moraines to explore the dynamic response of debris-covered glaciers to Holocene climatic change in the Khumbu Valley, Nepal Himalaya. *Journal of Geophysical Research - Earth Surface*, 127, e2022JF00664. Available from: <https://doi.org/10.1029/2022JF006645>
- Inoue, J. & Yoshida, M. (1980) Ablation and heat exchange over the Khumbu Glacier. *Seppyo*, 41, 26–33. Japanese Journal of Snow and Ice Special Issue.
- Inoue, J. (1977) Mass budget of Khumbu Glacier. *Seppyo*, 39(Special Issue), 15–19. Available from: [https://doi.org/10.5331/seppyo.39.Special\\_15](https://doi.org/10.5331/seppyo.39.Special_15)
- Iwata, S., Watanabe, O. & Fushimi, H. (1980) Surface morphology in the ablation area of the Khumbu Glacier. *Seppyo*, 41, 9–17. Japanese Journal of Snow and Ice Special Issue.
- Kaspari, S., Hooke, R.L.B., Mayewski, P.A., Kang, S.C., Hou, S.G. & Qin, D.H. (2007) Snow accumulation on Qomolangma (Mount Everest), Himalaya: synchronicity with sites across the Tibetan plateau on 50–100 year timescales. *Journal of Glaciology*, 54(185), 343–352. Available from: <https://doi.org/10.3189/002214308784886126>
- Kayastha, R.B. & Harrison, S.P. (2008) Changes in the equilibrium-line altitude since the Little Ice Age in the Nepalese Himalaya. *Annals of Glaciology*, 4(8), 93–99. Available from: <https://doi.org/10.3189/172756408784700581>
- Khadka, A., Matthews, T., Baker Perry, L., Koch, I., Wagnon, P., Shrestha, D., et al. (2021) Weather on Mount Everest during the 2019 summer monsoon. *Weather*, 76(6), 205–207. Available from: <https://doi.org/10.1002/wea.3931>
- King, O., Bhattacharya, A., Ghuffar, S., Tait, A., Guilford, S., Elmore, A.C., et al. (2020) Six decades of glacier mass changes around Mt. Everest are revealed by historical and contemporary images. *One Earth*, 3(5), 608–620. Available from: <https://doi.org/10.1016/j.oneear.2020.10.019>
- King, O., Quincey, D.J., Carrivick, J.L. & Rowan, A.V. (2017) Spatial variability in mass loss of glaciers in the Everest region, central Himalayas, between 2000 and 2015. *The Cryosphere*, 11(1), 407–426. Available from: <https://doi.org/10.5194/tc-11-407-2017>
- King, O., Turner, A.G.D., Quincey, D.J. & Carrivick, J.L. (2020) Morphometric evolution of Everest region debris-covered glaciers. *Geomorphology*, 371, 107422. Available from: <https://doi.org/10.1016/j.geomorph.2020.107422>
- Kirkbride, M.P. & Deline, P. (2013) The formation of supraglacial debris covers by primary dispersal from transverse englacial debris bands. *Earth Surface Processes and Landforms*, 38(15), 1779–1792. Available from: <https://doi.org/10.1002/esp.3416>
- Kirkbride, M.P. (1993) The temporal significance of transitions from melting to calving termini at glaciers in the central Southern Alps, New Zealand. *The Holocene*, 3(3), 232–240. Available from: <https://doi.org/10.1177/095968369300300305>
- Kristensen, L. & Benn, D.I. (2012) A surge of the glaciers Skobreen-Paulabreen, Svalbard, observed by time-lapse photographs and remote sensing data. *Polar Research*, 31(1), 11106. Available from: <https://doi.org/10.3402/polar.v31i0.11106>
- McClenaghan, M.B. & Paulen, R.C. (2018) Application of till mineralogy and geochemistry to mineral exploration. In: Menzies, J. & Van Der Meer, J.J.M. (Eds.) *Past glacial environments*, 2nd edition. Amsterdam: Elsevier, pp. 689–750.
- Miles, E.S., Watson, C.S., Brun, F., Berthier, E., Esteves, M., Quincey, D.J., et al. (2018) Glacial and geomorphic effects of a supraglacial lake drainage and outburst event, Everest region, Nepal Himalaya. *The Cryosphere*, 12(12), 3891–3905. Available from: <https://doi.org/10.5194/tc-12-3891-2018>
- Miles, K.E., Hubbard, B., Irvine-Flynn, T.D.L., Miles, E.S., Quincey, D.J. & Rowan, A.V. (2020) Hydrology of debris-covered glaciers in high-mountain Asia. *Earth Science Reviews*, 207, 103212. Available from: <https://doi.org/10.1016/j.earscirev.2020.103212>
- Miles, K.E., Hubbard, B., Quincey, D.J., Miles, E.S., Irvine-Flynn, T.D.L. & Rowan, A.V. (2019) Surface and subsurface hydrology of debris-covered Khumbu Glacier, Nepal, revealed by dye tracing. *Earth and Planetary Science Letters*, 513, 176–186. Available from: <https://doi.org/10.1016/j.epsl.2019.02.020>
- Moore, P.L. (2018) Stability of supraglacial debris. *Earth Surface Processes and Landforms*, 43(1), 285–297. Available from: <https://doi.org/10.1002/esp.4244>
- Moore, P.L. (2021) Numerical simulation of supraglacial debris stability: implications of ablation and landform genesis. *Frontiers in Earth Science*, 9, 710131. Available from: <https://doi.org/10.3389/feart.2021.710131>
- Murari, M.K., Owen, L.A., Dortch, J.M., Caffee, M.W., Dietsch, C., Fuchs, M., et al. (2014) Timing and climatic drivers for glaciation across monsoon-influenced regions of the Himalayan–Tibetan orogen. *Quaternary Science Reviews*, 88, 159–182. Available from: <https://doi.org/10.1016/j.quascirev.2014.01.013>
- Mölg, N., Ferguson, J., Bolch, T. & Vieli, A. (2020) On the influence of debris cover on glacier morphology: how high-relief structures evolve from smooth surfaces. *Geomorphology*, 357, 107092. Available from: <https://doi.org/10.1016/j.geomorph.2020.107092>
- Naito, N., Nakawo, M., Kadota, T. & Raymond, C. (2000) Numerical simulation of recent shrinkage of Khumbu Glacier, Nepal Himalayas. In: Nakawo, M., Raymond, C.F. & Fountain, A. (Eds.) *Debris-covered glaciers*, Vol. 264. Wallingford: IAHS Publication, pp. 245–254.
- Nakawo, M., Yabuki, H. & Sakai, A. (1999) Characteristics of Khumbu Glacier, Nepal Himalaya: recent change in the debris-covered area. *Annals of Glaciology*, 28, 118–122. Available from: <https://doi.org/10.3189/172756499781821788>
- Nuimura, T., Fujita, K., Yamaguchi, S. & Sharma, R.R. (2012) Elevation changes of glaciers revealed by multitemporal digital elevation models calibrated by GPS survey in the Khumbu region, Nepal Himalaya. *Journal of Glaciology*, 58(210), 648–656. Available from: <https://doi.org/10.3189/2012JG11J061>
- Owen, L.A., Finkel, R.C., Barnard, P.L., Haizhou, M., Asahi, K., Caffee, M.W., et al. (2005) Climatic and topographic controls on the style and timing of Late Quaternary glaciation throughout Tibet and the Himalaya defined by <sup>10</sup>Be cosmogenic radionuclide surface exposure dating. *Quaternary Science Reviews*, 24(12–13), 1391–1411. Available from: <https://doi.org/10.1016/j.quascirev.2004.10.014>
- Owen, L.A., Robinson, R., Benn, D.I., Finkel, R.C., Davis, N.K., Yi, C., et al. (2009) Quaternary glaciations of Mount Everest. *Quaternary Science Reviews*, 28(15–16), 1412–1433. Available from: <https://doi.org/10.1016/j.quascirev.2009.02.010>
- Quincey, D.J., Luckman, A. & Benn, D. (2009) Quantification of Everest region glacier velocities between 1992 and 2002, using satellite radar interferometry and feature tracking. *Journal of Glaciology*, 55(192), 596–606. Available from: <https://doi.org/10.3189/002214309789470987>
- Rowan, A.V. (2017) The ‘Little Ice Age’ in the Himalaya: a review of glacier advance driven by Northern Hemisphere temperature change. *The Holocene*, 27(2), 292–308. Available from: <https://doi.org/10.1177/0959683616658530>
- Rowan, A.V., Egholm, D.L., Quincey, D.J. & Glasser, N.F. (2015) Modelling the feedbacks between mass balance, ice flow and debris transport to predict the response to climate change of debris-covered glaciers in the Himalaya. *Earth and Planetary Science Letters*, 430, 427–438. Available from: <https://doi.org/10.1016/j.epsl.2015.09.004>
- Rowan, A.V., Egholm, D.L., Quincey, D.J., Hubbard, B., King, O., Miles, E.S., et al. (2021) The role of differential ablation and dynamic detachment in driving accelerating mass loss from a debris-covered Himalayan glacier. *Journal of Geophysical Research - Earth Surface*, 126, e2020JF005761. Available from: <https://doi.org/10.1029/2020JF005761>



- Rupper, S., Roe, G. & Gillespie, A. (2009) Spatial patterns of Holocene glacier advance and retreat in Central Asia. *Quaternary Research*, 72(3), 337–346. Available from: <https://doi.org/10.1016/j.yqres.2009.03.007>
- Sakai, A., Takeuchi, N., Fujita, K. & Nakawo, M. (2000) Role of supraglacial ponds in the ablation process of a debris covered glacier in the Nepal Himalayas. In: Nakawo, M., Raymond, C.F. & Fountain, A. (Eds.) *Debris-covered glaciers*, Vol. 264. Wallingford: IAHS Publication, pp. 119–132.
- Scherler, D. & Egholm, D.L. (2020) Production and transport of supraglacial debris: insights from cosmogenic  $^{10}\text{Be}$  and numerical modelling, Chhota Shigri Glacier, Indian Himalaya. *Journal of Geophysical Research - Earth Surface*, 125, e2020JF005586. Available from: <https://doi.org/10.1029/2020JF005586>
- Scherler, D. (2014) Climatic limits to headwall retreat in the Khumbu Himalaya, eastern Nepal. *Geology*, 42(11), 1019–1022. Available from: <https://doi.org/10.1130/G35975.1>
- Scherler, D., Bookhagen, B. & Strecker, M.R. (2011) Hillslope-glacier coupling: the interplay of topography and glacial dynamics in High Asia. *Journal of Geophysical Research*, 116, F02019. Available from: <https://doi.org/10.1029/2020JF001751>
- Scherler, D., LePrince, S. & Strecker, M.R. (2008) Glacier surface velocities in alpine terrain from optical satellite imagery—accuracy improvement and quality assessment. *Remote Sensing of Environment*, 112(10), 3806–3819. Available from: <https://doi.org/10.1016/j.rse.2008.05.01>
- Searle, M., Simpson, R.L., Law, R.D., Parrish, R.R. & Waters, D.J. (2003) The structural geometry, metamorphic and magmatic evolution of the Everest massif, High Himalaya of Nepal-South Tibet. *Journal of the Geological Society of London*, 160(3), 345–366. Available from: <https://doi.org/10.1144/0016-764902-126>
- Seko, K., Yabuki, H., Nakawo, M., Sakai, A., Kadota, T. & Yamada, Y. (1998) Changing surface features of Khumbu glacier, Nepal Himalayas, revealed by SPOT images. *Bulletin of Glacier Research*, 16, 33–41.
- Shean, D. (2017) *High Mountain Asia 8-meter DEM mosaics derived from optical imagery, version 1*, Boulder, Colorado USA. National Snow and Ice Data Center: NASA.
- Sherriff, S., Franks, S.W., Rowan, J.S., Fenton, Ó. & Ó'hUallacháin, D. (2015) Uncertainty-based assessment of tracer selection, tracer non-conservativeness and multiple solutions in sediment fingerprinting using synthetic and field data. *Journal of Soils and Sediments*, 15(10), 2101–2116. Available from: <https://doi.org/10.1007/s11368-015-1123-5>
- Sherriff, S., Rowan, J.S., Fenton, O., Jordan, P. & Ó'hUallacháin, D. (2018) Sediment fingerprinting as a tool to identify temporal and spatial variability of sediment sources and transport pathways in agricultural catchments. *Agriculture, Ecosystems and Environment*, 267, 188–200. Available from: <https://doi.org/10.1016/j.agee.2018.08.023>
- Small, R.J. & Clark, M.J. (1974) The medial moraines of the lower glacier de Tsidiore Neuve, Valais, Switzerland. *Journal of Glaciology*, 13(68), 255–263. Available from: <https://doi.org/10.3189/S0022143000023066>
- Stephens, G.C., Evenson, E.B. & Detra, D.E. (1990) A geochemical sampling technique for use in areas of active alpine glaciation: an application from the central Alaska Range. *Journal of Geochemical Exploration*, 37(3), 301–321. Available from: [https://doi.org/10.1016/0375-6742\(90\)90105-J](https://doi.org/10.1016/0375-6742(90)90105-J)
- Thakuri, S., Salerno, E., Smiraglia, C., Bolch, T., D'Agata, C., Viviano, G., et al. (2014) Tracing glacier changes since the 1960s on the south slope of Mt Everest (central Southern Himalaya) using optical satellite imagery. *The Cryosphere*, 8(4), 1297–1315. Available from: <https://doi.org/10.5194/tc-8-1297-2014>
- Ward, D.J. & Anderson, R.S. (2011) The use of ablation-dominated medial moraines as samplers for  $^{10}\text{Be}$ -derived erosion rates of glacier valley walls, Kichatna Mountains, AK. *Earth Surface Processes and Landforms*, 36(4), 495–512. Available from: <https://doi.org/10.1002/esp.2068>
- Ward, M.P. & Clark, P.K. (1992) Everest 1951: cartographic and photographic evidence of a new route from Nepal. *Geographical Journal*, 158(1), 47–56. Available from: <https://doi.org/10.2307/3060016>
- Watson, C.S., Quincey, D.J., Carrivick, J.L. & Smith, M.W. (2016) The dynamics of supraglacial ponds in the Everest region, central Himalaya. *Global and Planetary Change*, 142, 14–27. Available from: <https://doi.org/10.1016/j.gloplacha.2016.04.008>
- Westoby, M.J., Rounce, D.R., Shaw, T.E., Fyfe, C.L., Moore, P.L., Stewart, R.L., et al. (2020) Geomorphological evolution of a debris-covered glacier surface. *Earth Surface Processes and Landforms*, 45(14), 3431–3448. Available from: <https://doi.org/10.1002/esp.4973>
- Wetterauer, K., Scherler, D., Anderson, L.S. & Wittman, H. (2022) Temporal evolution of headwall erosion rates derived from cosmogenic nuclide concentrations in the medial moraines of Glacier d'Otemma, Switzerland. *Earth Surface Processes and Landforms*, 47(10), 2437–2454. Available from: <https://doi.org/10.1002/esp.5386>

## SUPPORTING INFORMATION

Additional supporting information can be found online in the Supporting Information section at the end of this article.

**How to cite this article:** Kirkbride, M.P., Sherriff, S.C., Rowan, A.V., Egholm, D.L., Quincey, D.J., Miles, E. et al. (2023) Provenance and transport of supraglacial debris revealed by variations in debris geochemistry on Khumbu Glacier, Nepal Himalaya. *Earth Surface Processes and Landforms*, 1–17. Available from: <https://doi.org/10.1002/esp.5657>